



# *In operando* quantitation of Li concentration for a commercial Li-ion rechargeable battery using high-energy X-ray Compton scattering

Kosuke Suzuki,<sup>a\*</sup> Ayahito Suzuki,<sup>a</sup> Taiki Ishikawa,<sup>a</sup> Masayoshi Itou,<sup>b</sup> Hisao Yamashige,<sup>c</sup> Yuki Orikasa,<sup>d</sup> Yoshiharu Uchimoto,<sup>e</sup> Yoshiharu Sakurai<sup>b</sup> and Hiroshi Sakurai<sup>a</sup>

Received 10 May 2017

Accepted 7 July 2017

Edited by P. A. Pianetta, SLAC National Accelerator Laboratory, USA

**Keywords:** Li-ion battery; *in operando* measurement; quantitation; Compton profile.

**Supporting information:** this article has supporting information at journals.iucr.org/s

<sup>a</sup>Department of Electronics and Informatics, Gunma University, 1-5-1 Tenjin-cho, Kiryu, Gunma 376-8515, Japan, <sup>b</sup>Japan Synchrotron Radiation Research Institute (JASRI), 1-1-1 Kouto, Sayo, Hyogo 679-5198, Japan, <sup>c</sup>Material Platform Engineering Division, Toyota Motor Corporation, 1 Toyota-cho, Toyota, Aichi 471-8572, Japan, <sup>d</sup>Department of Applied Chemistry, Ritsumeikan University, 1-1-1 Noji-higashi, Kusatsu, Shiga 525-8577, Japan, and <sup>e</sup>Graduate School of Human and Environmental Studies, Kyoto University, Sakyo, Kyoto 606-8501, Japan.

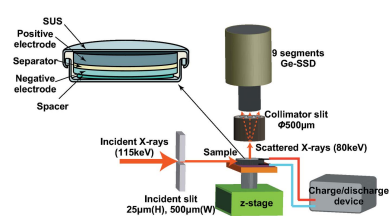
\*Correspondence e-mail: kosuzuki@gunma-u.ac.jp

Compton scattering is one of the most promising probes for quantitating Li under *in operando* conditions, since high-energy X-rays, which have high penetration power, are used as the incident beam and the Compton-scattered energy spectrum has specific line-shapes for each element. An *in operando* quantitation method to determine the Li composition in electrodes has been developed by using line-shape (S-parameter) analysis of the Compton-scattered energy spectrum. In this study, S-parameter analysis has been applied to a commercial coin cell Li-ion rechargeable battery and the variation of the S-parameters during the charge/discharge cycle at the positive and negative electrodes has been obtained. By using calibration curves for Li composition in the electrodes, the change in Li composition of the positive and negative electrodes has been determined using the S-parameters simultaneously.

## 1. Introduction

*In operando* quantitation of Li ions, which contribute to electrode reactions, is crucially important for producing high-performance Li-ion rechargeable batteries with high efficiency, high safety and long lifetime. Generally, the electrodes of a Li-ion battery are made from several compounds: active material, a conductive aid and binder. With such electrodes, therefore, it has been reported that inhomogeneous electrode reactions occur (Nishi *et al.*, 2013). These inhomogeneous reactions induce an overvoltage by repeating the charge/discharge cycle. It is important to monitor the Li-ion distribution in the electrodes in order to understand where the overvoltage state is made. Although the development of experimental techniques to visualize Li distributions has attracted much attention, these experimental methods have been mainly adopted for the positive electrode (Liu *et al.*, 2010; Mima *et al.*, 2012; Wang *et al.*, 2014; Jensen *et al.*, 2015; He *et al.*, 2015). Reactions over the whole battery have been observed using neutron sources; however, the spatial resolution is limited compared with using X-ray sources (Wang *et al.*, 2012).

So far, we have been investigating the mechanism of electrode reactions in positive electrode materials, *i.e.*  $\text{Li}_x\text{Mn}_2\text{O}_4$ ,  $\text{Li}_x\text{CoO}_2$  and  $\text{Li}_x\text{FePO}_4$  (Suzuki *et al.*, 2015; Barbiellini *et al.*, 2016; Hafiz *et al.*, 2017), and developing *in operando* quanti-



© 2017 International Union of Crystallography

tation methods for Li ions using high-energy X-ray Compton scattering spectroscopy. Merits of the Compton scattering technique include experiments yielding bulk observations on working batteries, since X-ray photons of >100 keV can be used as the incident beam which can penetrate deep into materials, including closed electrochemical cells, and the Compton-scattered energy spectrum, the so-called Compton profile, having a specific line-shape for each element. In a previous study we developed a method to quantify the Li concentration by introducing the shape parameter (*S*-parameter) of the Compton profile. In a Compton profile, the contribution from the Li concentration clearly appears. The *S*-parameter is a parameter that digitalizes the line-shape of a Compton profile. By using the *S*-parameter, we confirmed that the experimental *S*-parameters obtained from polycrystalline  $\text{Li}_x\text{Mn}_2\text{O}_4$  pellets are proportional to the Li composition of the samples obtained from inductively coupled plasma (ICP) analysis. Moreover, we successfully observed non-destructively the change of Li concentration of a commercial CR2032 coin battery using the *S*-parameters (Suzuki *et al.*, 2016). However, this Li concentration was obtained from only the positive electrode. Hence, in this study, we applied *S*-parameter analysis to a commercial Li-ion secondary battery, VL2020, and observed the Li concentration including the positive and negative electrodes during the charge/discharge cycle.

## 2. Experiment and data analysis

A coin cell Li-ion rechargeable battery, VL2020, made by Panasonic Corporation, was used for the Compton profile measurements. The VL2020 comprises a  $\text{V}_2\text{O}_5$  positive electrode of thickness 800  $\mu\text{m}$ , a LiAl alloy negative electrode of  $\sim 300 \mu\text{m}$  thickness, an olefin-based non-woven fabric separator, Al wire-netting spacer and dimethoxyethane electrolyte, as shown in Fig. 1. Compton scattering experiments were performed at the BL08W beamline at the SPring-8 synchrotron facility, Japan. Fig. 1 shows the experimental setup of the Compton scattering experiment. Synchrotron radiation emitted from an elliptical multipole wiggler was used as the incident X-rays. The incident X-ray energy was tuned to

115 keV by an asymmetric Johann-type Si(400) monochromator. The incident X-rays, of 25  $\mu\text{m}$  height and 500  $\mu\text{m}$  width after passing through an incident slit, were delivered to the coin battery. The Compton-scattered X-ray intensities were measured by using a nine-segment Ge solid-state detector (SSD). A collimator slit of diameter 500  $\mu\text{m}$  was arranged between the sample and the detector. The scattering angle was fixed at 90°. The probing volume for the measurement was determined by the incident and collimator slits to be 25  $\mu\text{m} \times 500 \mu\text{m} \times 500 \mu\text{m}$ . The coin battery was connected to a charge/discharge device (HZ7000, Hokuto Denko Corporation) and the charge state of the battery was changed by charging or discharging at a 0.4 C rate. The Li concentrations for the fully charged state (state of charge: SOC100) and fully discharged state (SOC0) of the positive and negative electrodes were confirmed by ICP analysis at the Center for Instrumental Analysis of Gunma University.

By measuring the Compton scattered X-ray energy spectrum we can obtain the Compton profile. The Compton profile,  $J(p_z)$ , is defined by following equation (Cooper *et al.*, 2004),

$$J(p_z) = \iint \rho(\mathbf{p}) dp_x dp_y, \quad (1)$$

where  $\rho(\mathbf{p})$  is the electron momentum density,  $\mathbf{p} = (p_x, p_y, p_z)$  is the momentum and  $p_z$  is taken to lie along the direction of the scattering vector.  $\rho(\mathbf{p})$  is given by the following equation (Barbiellini & Bansil, 2001; Barbiellini, 2000),

$$\rho(\mathbf{r}) = \sum_j n_j \left| \int \Psi_j(\mathbf{r}) \exp(-i\mathbf{p} \cdot \mathbf{r}) d\mathbf{r} \right|^2, \quad (2)$$

where  $\Psi_j(\mathbf{r})$  is the wavefunction of an electron in the *j*-state and  $n_j$  is the corresponding electron occupation. The index *j* runs over all constituent atoms and orbitals. The line-shape of a Compton profile varies depending on each element because the Compton profile directly links to wavefunction of the electron. The *S*-parameter is defined as

$$S = \frac{S_L}{S_H} = \frac{\int_{-d}^d J(p_z) dp_z}{\int_{-r}^r J(p_z) dp_z + \int_d^r J(p_z) dp_z}, \quad (3)$$

where  $S_L$  and  $S_H$  are the areas under the Compton profile covering the low- and high-momentum regions. The parameters *d* and *r* are the range of the low-momentum and high-momentum regions, respectively. In this study, *d* = 1 atomic units (a.u.) and *r* = 5 a.u. are used. Details of the decision method used to determine the parameters *d* and *r* are given in the supporting information.

## 3. Results and discussion

Fig. 2(a) shows energy spectra for stainless steel (SUS), the positive electrode, separator and negative electrode. In order to compare the line-shapes of these energy spectra, the area of each spectrum is normalized to the same value. In Fig. 2(a),

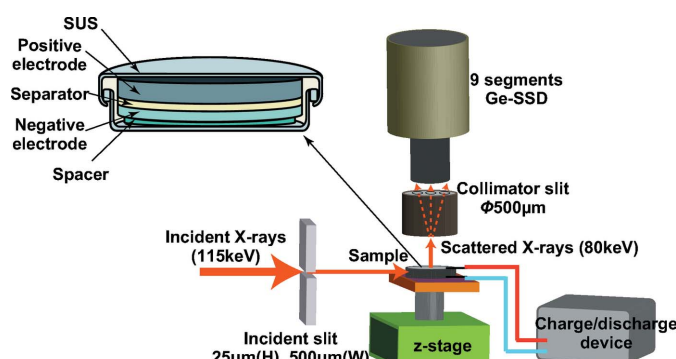


Figure 1

Experimental setup of the Compton scattering experiment at BL08W of SPring-8 and configuration of the coin battery VL2020.

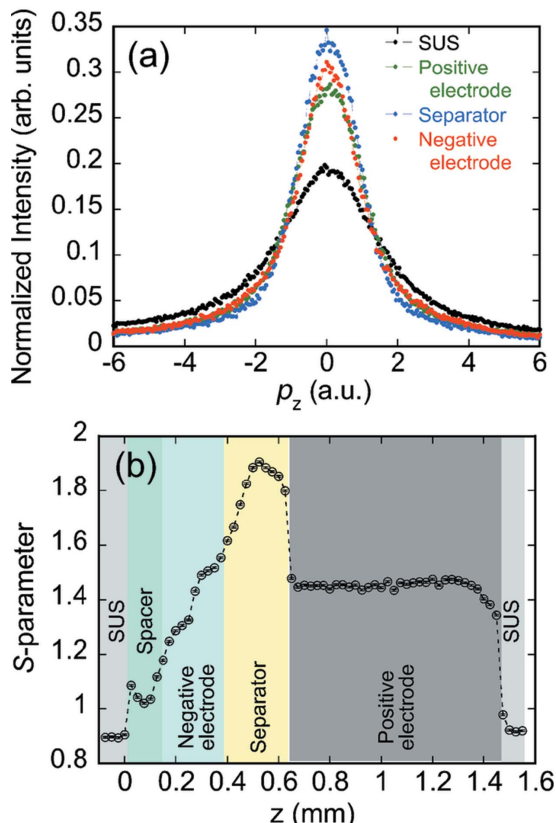


Figure 2

(a) Compton-scattered energy spectrum for SUS (black dots), the positive electrode (green dots), separator (blue dots) and negative electrode (red dots). In order to compare the line-shapes of the spectra, the area of each spectrum was normalized to the same value. (b) Battery component through  $S$ -parameters. On the  $x$ -axis,  $z$  corresponds to the  $z$  direction of the battery.

the energy spectrum for the separator has the sharpest line-shape and the energy spectrum for SUS has the broadest line-shape. Therefore, the  $S$ -parameter obtained from the separator energy spectrum has the highest value. On the other hand, the  $S$ -parameter obtained from the SUS energy spectrum has the smallest value.  $S$ -parameters which were obtained by scanning the incident X-rays along the vertical ( $z$ ) direction of the battery are shown in Fig. 2(b). In this figure, the region  $z < 0$  mm and  $1.5$  mm  $< z$  corresponds to the battery outer case (SUS), region  $0$  mm  $< z < 0.15$  mm to the spacer (Al wire-netting), region  $0.15$  mm  $< z < 0.4$  mm to the negative electrode (LiAl), region  $0.4$  mm  $< z < 0.65$  mm to the separator, and region  $0.65$  mm  $< z < 1.5$  mm to the positive electrode ( $V_2O_5$ ). The structure in the VL2020 battery is revealed through the  $S$ -parameters.

We measured the Compton-scattered X-ray energy spectrum by scanning the incident X-rays along the  $z$  direction on the battery while changing the state of charge (SOC). The charge–discharge curve for this measurement is shown in Fig. 3(a). The initial voltage is 3.507 V. The full charged state voltage is 3.5 V and the full discharged state voltage is 2.5 V. The SOC is changed every 2.5 h by a constant current of 8 mA. There is a rest time of 30 min between the first discharge and the first charge and between the first charge and the second

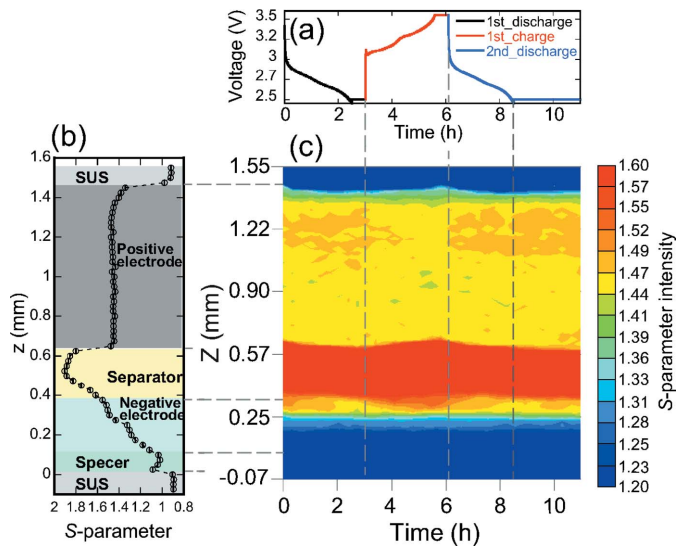


Figure 3

(a) Charge/discharge curve of VL2020. ‘1st discharge’, ‘1st charge’ and ‘2nd discharge’ correspond to the black, red and blue solid lines, respectively. (b) Components of the battery. (c)  $S$ -parameter distribution during the charge/discharge cycle.

discharge. After the second discharge, battery reactions were relaxed for 3 h. The  $z$  position scan with 66 steps was repeated 34 times for 11.6 h to obtain the  $S$ -parameter distribution. The measurement time was 15 s at one data point. The  $z$  value of the  $y$ -axis corresponds to the vertical position of the battery, as shown in Fig. 3(b). The  $S$ -parameter distribution obtained from the Compton-scattered X-ray energy spectrum is shown in Fig. 3(c). The color distribution corresponds to the  $S$ -parameter intensity. Variations of the  $S$ -parameters appear at the upper area of the positive electrode (around  $z = 1.22$  mm) and at the interface between the separator and negative electrode (around  $z = 0.3$  mm). Moreover, we observed that the separator position moves towards the positive electrode during charge and returns to the initial position during discharge. It is thought that this migration of the separator position is induced by expansion or contraction of the lattice volume in the negative electrode. The volume expansion from Al to LiAl is 95% (Morales *et al.*, 2010); on the other hand, the volume expansion from  $V_2O_5$  to  $Li_{0.5}V_2O_5$  is 2.2% (Voikov *et al.*, 1994; Wächter *et al.*, 2014).

In order to quantify the change of the  $S$ -parameters during the charge/discharge cycle, the separator position was corrected. The correction, which assumed a volume expansion in the negative electrode, was performed by using following equation,

$$z_c = az_i^2 + bz_i. \quad (4)$$

Here,  $z_c$  and  $z_i$  are the corrected and initial  $z$  position of the battery, respectively. The coefficients  $a$  and  $b$  are determined by the least-squares method.

Fig. 4 shows the difference  $S$ -parameter ( $\Delta S$ ) distribution during the charge/discharge process.  $\Delta S$  is defined as

$$\Delta S = S_t - S_0. \quad (5)$$

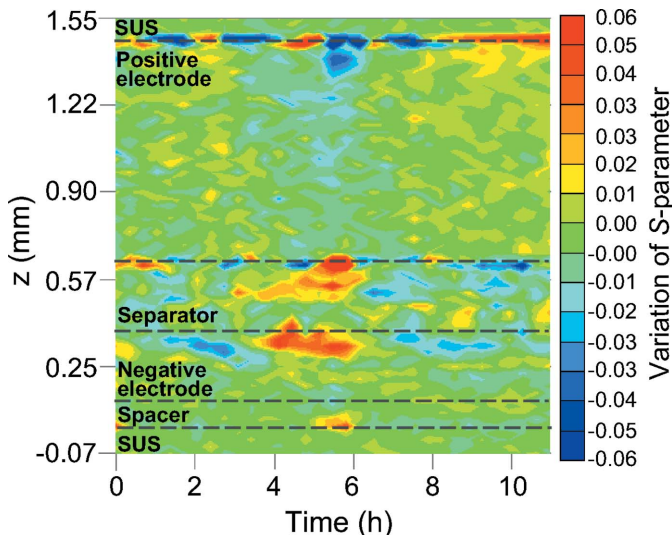


**Figure 4**  
Variation of the S-parameter distribution.

Here,  $S_t$  is the S-parameter at  $t$  seconds, and  $S_0$  is the averaged S-parameter over the whole measurement time at each  $z$  position. From Fig. 4, it seems that the S-parameters at the positive electrode increase during discharge and decrease during charge homogeneously. On the other hand, variations of the S-parameters at the negative electrode mostly appear at the interface between the negative electrode and the separator. In a previous study we confirmed that there is a linear relation between the S-parameters and Li concentration (Suzuki *et al.*, 2016). Hence, we can think that the variation of the S-parameter in the positive and negative electrodes during the charge/discharge cycle corresponds to the change of Li concentration. This indicates that inhomogeneous lithium reactions easily occur in the negative electrode. We observe a change of the S-parameters in the separator region as well. In order to consider this S-parameter change in the separator region, raw S-parameter data from the separator region are shown in Fig. 5. By charging the battery, the value of the S-parameter increases, then returns to its initial value by discharge. This indicates that some Li ions remain in the separator when the Li ions move from the positive electrode to the negative electrode by the charge cycle. One possible reason for this is that the residue of the Li ions induces a capacity loss in the battery.

Fig. 6 shows the average of the S-parameters during charge/discharge for the positive and negative electrodes. The averaged S-parameter variations are obtained from the S-parameters of each scan at the positive and negative electrodes regions in Fig. 3(c). The S-parameters decrease by 0.92% in the positive electrode from discharge to charge and increase by 1.69% in the negative electrode from discharge to charge. In order to quantitate the Li concentration,  $x$ , from the S-parameters, the theoretical S-parameters of  $\text{Li}_x\text{V}_2\text{O}_5$  ( $x = 0, 0.124, 0.25, 0.5, 0.75$  and 1) and  $\text{Li}_x\text{Al}$  ( $x = 0, 0.046, 0.25, 0.5, 0.75$  and 1) were calculated using atomic model Compton profile data (Biggs *et al.*, 1975). As Li composition reference data, ICP analysis was performed for the positive and negative

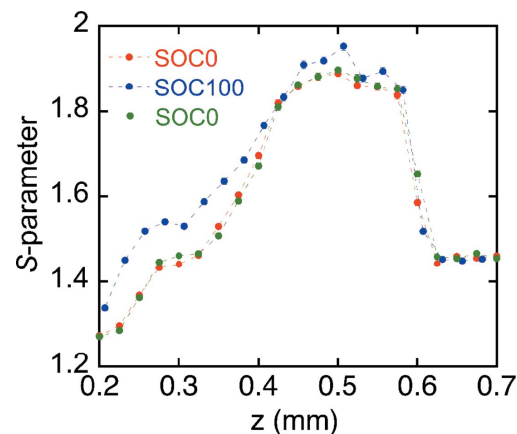


**Figure 5**  
Raw S-parameter data at the separator region. Red and green dots show data obtained by the first discharge and second discharge, respectively, and blue dots show data obtained by the first charge of the battery.

electrodes at SOC100 and SOC0. The mass of Li at SOC100 is  $1.497 \text{ mg l}^{-1}$  in the positive electrode and  $5.068 \text{ mg l}^{-1}$  in the negative electrode, and at SOC0 is  $5.373 \text{ mg l}^{-1}$  in the positive electrode and  $1.211 \text{ mg l}^{-1}$  in the negative electrode. The molar ratio of Li,  $x$ , is calculated using

$$x = \frac{M_{\text{VO}} m_{\text{Li}}}{M_{\text{Li}} m_{\text{LVO}}} \quad (\text{positive electrode}), \quad (6)$$

$$x = \frac{M_{\text{A}} m_{\text{Li}}}{M_{\text{Li}} m_{\text{LA}}} \quad (\text{negative electrode}).$$

Here,  $M_{\text{VO}}$  ( $= 181.878$ ) is the molecular weight for  $\text{V}_2\text{O}_5$ .  $M_{\text{A}}$  ( $= 26.982$ ) and  $M_{\text{Li}}$  ( $= 6.941$ ) are the atomic weights for Al and Li atoms, respectively.  $m_{\text{LVO}}$ ,  $m_{\text{LA}}$  and  $m_{\text{Li}}$  are the mass of  $\text{Li}_x\text{V}_2\text{O}_5$ ,  $\text{Li}_x\text{Al}$  and Li, respectively.  $m_{\text{LVO}}$  and  $m_{\text{LA}}$  of SOC100 and SOC0 were measured by using an electronic balance. The values of  $\text{Li}_x\text{V}_2\text{O}_5$  are 330.7 mg at SOC0 and 317.4 mg at

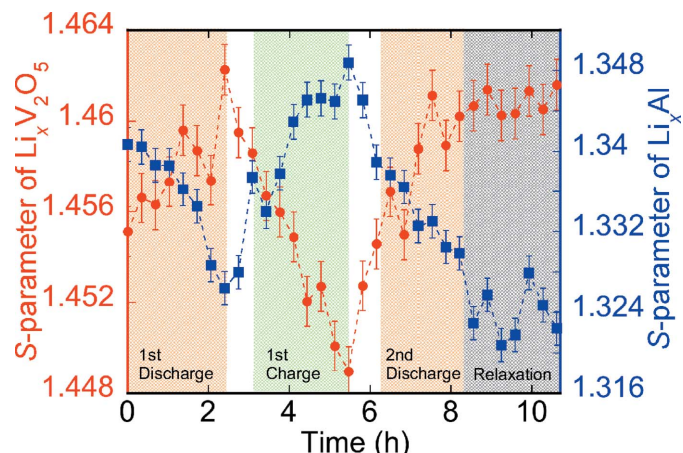


**Figure 6**  
Variation of the S-parameters during the charge/discharge cycle in the  $\text{Li}_x\text{V}_2\text{O}_5$  positive electrode material (red dots) and  $\text{Li}_x\text{Al}$  negative electrode material (blue squares). Orange background color regions correspond to the first discharge and second discharge, respectively. Green and gray background color regions correspond to the first charge and relaxation, respectively.

SOC100, and of Li<sub>x</sub>Al are 103.0 mg at SOC0 and 110.6 mg at SOC100. The values obtained from ICP analysis were used as  $m_{\text{Li}}$ . The obtained lithium composition of Li<sub>x</sub>V<sub>2</sub>O<sub>5</sub> is 0.426 at SOC0 and 0.124 at SOC100, and of Li<sub>x</sub>Al is 0.046 at SOC0 and 0.178 at SOC100, respectively. Since the momentum resolution and background are different between the experimental and theoretical data, the theoretical *S*-parameters of Li<sub>0.124</sub>V<sub>2</sub>O<sub>5</sub> are normalized by the experimental value of the *S*-parameter at SOC100. Similarly, the theoretical *S*-parameters of Li<sub>0.046</sub>Al are normalized by the experimental value of the *S*-parameter at SOC0. Figs. 7(a) and 7(b) show the calibration curves for Li<sub>x</sub>V<sub>2</sub>O<sub>5</sub> and Li<sub>x</sub>Al, which are  $y = 32.609x - 47.186$  in Li<sub>x</sub>V<sub>2</sub>O<sub>5</sub> and  $y = 5.299x - 6.967$  in Li<sub>x</sub>Al, respectively. By using these calibration curves, the Li compositions,  $x$ , for SOC0 in the positive electrode and for SOC100 in the negative electrode are obtained as  $x = 0.470 \pm 0.012$  and  $x = 0.170 \pm 0.006$ , respectively. These values are equal to the values obtained from the ICP analysis. Fig. 8 shows the variation of the Li composition in Li<sub>x</sub>V<sub>2</sub>O<sub>5</sub> and Li<sub>x</sub>Al during the charge/discharge cycle. These Li compositions were obtained by applying calibration curves to the data of Fig. 6. We successfully quantitated the Li concentration of the positive and negative electrodes in a commercial Li-ion rechargeable battery during the charge/discharge cycle simultaneously.

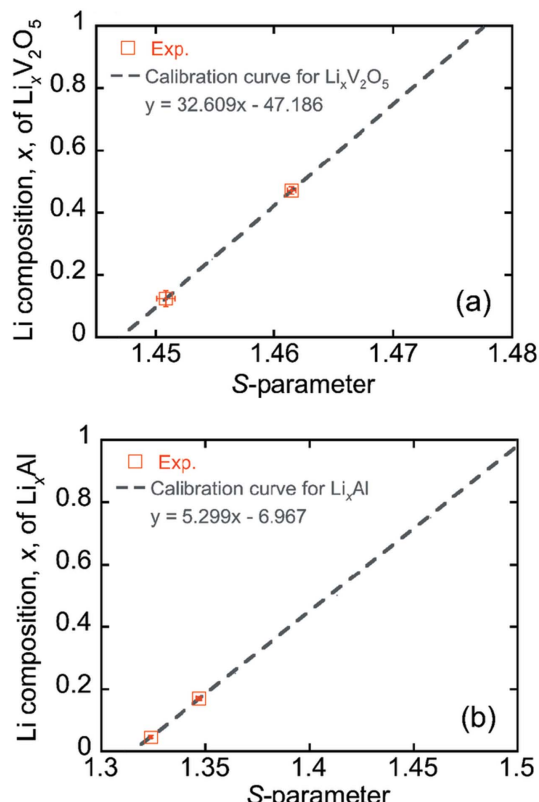


Figure 7

Calibration curves for Li<sub>x</sub>V<sub>2</sub>O<sub>5</sub> and Li<sub>x</sub>Al calculated by using the atomic model Compton profile. The theoretical *S*-parameters for Li<sub>0.124</sub>V<sub>2</sub>O<sub>5</sub> are normalized by the value of the experimental *S*-parameter at SOC100 in the positive electrode. The theoretical *S*-parameters for Li<sub>0.046</sub>Al are normalized by the value of experimental *S*-parameter at SOC0 in the negative electrode.

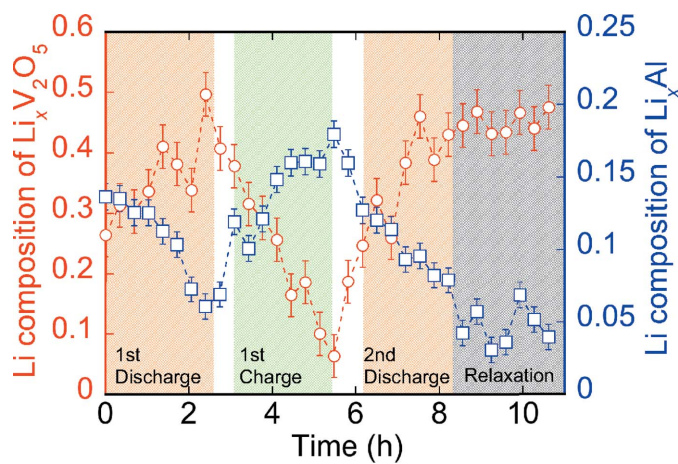


Figure 8

Change of Li composition obtained from the calibration curve during charge/discharge cycle. Red dots and blue dots correspond to the Li concentration in the Li<sub>x</sub>V<sub>2</sub>O<sub>5</sub> positive electrode material and Li<sub>x</sub>Al negative electrode material, respectively. Orange background color regions correspond to the first discharge and second discharge, respectively. Green and gray background color regions correspond to first charge and relaxation, respectively.

#### 4. Summary

In this study, we applied *S*-parameter analysis of Compton-scattered energy spectra to a commercial coin cell Li-ion rechargeable battery, VL2020. The structure of VL2020 was revealed by the *S*-parameters. The *S*-parameter distribution corresponding to the charge/discharge cycle is obtained at the positive and negative electrodes. When the battery was charged, the migration of the separator position induced by lattice expansion of the negative electrode was observed. By using calibration curves obtained from theoretical *S*-parameters, we obtained the Li concentration of the positive and negative electrodes during the charge/discharge cycle simultaneously.

#### Acknowledgements

The authors thank Mr K. Iwamaru, Professor F. Hayashi and Professor K. Tsunoda of Gunma University for technical support during the ICP measurements. This work was supported by Japan Science and Technology Agency, and Grant-in-Aid for Young Scientists (B) from MEXT KAKENHI under grant Nos. 24750065 and 15K17873. The Compton scattering experiments were performed with the approval of JASRI [proposal Nos. 2013A1007, 2013B1019, 2014A1012, 2014B1023, 2015A1010, 2015A1477, 2015B1010, 2015B1213, 2016A1016, 2016A1211 and 2016B1020].

#### Funding information

The following funding is acknowledged: Japan Science and Technology Agency; Ministry of Education, Culture, Sports, Science and Technology (award No. 24750065; award No. 15K17873).

## References

- Barbiellini, B. (2000). *J. Phys. Chem. Solids*, **61**, 341–344.
- Barbiellini, B. & Bansil, A. (2001). *J. Phys. Chem. Solids*, **62**, 2181–2189.
- Barbiellini, B., Suzuki, K., Orikasa, Y., Kaprzyk, S., Itou, M., Yamamoto, K., Wang, Y. J., Hafiz, H., Yamada, R., Uchimoto, Y., Bansil, A., Sakurai, Y. & Sakurai, H. (2016). *Appl. Phys. Lett.* **109**, 073102.
- Biggs, F., Mendelsohn, L. B. & Mann, J. B. (1975). *At. Data Nucl. Data Tables*, **16**, 201–309.
- Cooper, M. J., Mijnarends, P. E., Shiotani, N., Sakai, N. & Bansil, A. (2004). *X-ray Compton Scattering*, pp. 31–39. Oxford University Press.
- Hafiz, H., Suzuki, K., Barbiellini, B., Orikasa, Y., Callewaert, V., Kaprzyk, S., Itou, M., Yamamoto, K., Yamada, R., Uchimoto, Y., Sakurai, Y., Sakurai, H. & Bansil, A. (2017). *Sci. Adv.* To be published.
- He, H., Liu, B., Abouimrane, A., Ren, Y., Liu, Y., Liu, Q. & Chao, Z. S. (2015). *J. Electrochem. Soc.* **162**, A2195–A2200.
- Jensen, K. M. O., Yang, X., Laveda, J. V., Zeier, W. G., See, K. A., Michiel, M. D., Melot, B. C., Corr, S. A. & Billinge, S. J. L. (2015). *J. Electrochem. Soc.* **162**, A1310–A1314.
- Liu, J., Kunz, M., Chen, K., Tamura, N. & Richardson, T. J. (2010). *J. Phys. Chem. Lett.* **1**, 2120–2123.
- Mima, K., Gonzalez-Arrabal, R., Azuma, H., Yamazaki, A., Okuda, C., Ukyo, Y., Sawada, H., Fujita, K., Kato, Y., Perlado, J. M. & Nakai, S. (2012). *Methods Phys. Res. B*, **290**, 79–84.
- Morales, J., Trócoli, R., Franger, S. & Santos-Peña, J. (2010). *Electrochim. Acta*, **55**, 3075–3082.
- Nishi, T., Nakai, H. & Kita, A. (2013). *J. Phys. Chem. Lett.* **160**, A1785–A1788.
- Suzuki, K., Barbiellini, B., Orikasa, Y., Go, N., Sakurai, H., Kaprzyk, S., Itou, M., Yamamoto, K., Uchimoto, Y., Wang, Y. J., Hafiz, H., Bansil, A. & Sakurai, Y. (2015). *Phys. Rev. Lett.* **114**, 087401.
- Suzuki, K., Barbiellini, B., Orikasa, Y., Kaprzyk, S., Itou, M., Yamamoto, K., Wang, Y. J., Hafiz, H., Uchimoto, Y., Bansil, A., Sakurai, Y. & Sakurai, H. (2016). *J. Appl. Phys.* **119**, 025103.
- Voikov, V. L., Zakharova, G. S. & Kuznetsov, M. V. (1994). *Ross. J. Inorg. Chem.* **39**, 1808–1813.
- Wächter, F., Krumeich, F. & Nesper, R. (2014). *Chem. Eur. J.* **20**, 5202–5208.
- Wang, J., Chen-Wiegart, Y. C. & Wang, J. (2014). *Nat. Commun.* **5**, 4570.
- Wang, X. L., An, K., Cai, L., Feng, Z., Nagler, S. E., Daniel, C., Rhodes, K. J., Stoica, A. D., Skorpenske, H. D., Liang, C., Zhang, W., Kim, J., Qi, Y. & Harris, S. J. (2012). *Sci. Rep.* **2**, 747.